Two-point correlations conditioned on the turbulent/non-turbulent interface in a turbulent temporal jet

J.-P. Mollicone*

Department of Mechanical Engineering, Faculty of Engineering, University of Malta, Msida MSD 2080, Malta

A. Cimarelli

DIEF, University of Modena and Reggio Emilia, 41125 Modena, Italy

E. De Angelis

DIN, Università di Bologna, Forli, 47121, Italy

School of Engineering, Cardiff University, Cardiff CF24 3AA, UK

M. van Reeuwijk

Department of Civil and Environmental Engineering, Imperial College London, London SW7 2AZ, United Kingdom

(Dated: January 20, 2026)

Abstract

The paper investigates one- and two-point correlations conditioned to the turbulent/non-turbulent interface (TNTI) of a planar turbulent temporal jet. A classical average, which is taken with respect to a spatially averaged TNTI location, is compared to two types of conditional averages, which are conditioned with respect to the instantaneous TNTI. We show that the two conditional averages differ from the classical average, especially in the TNTI region and over a distance which is comparable to the standard deviation of the instantaneous TNTI location. All correlations scale in a self-similar manner with time when normalised with a characteristic jet width calculated from integral quantities of momentum and volume fluxes. The paper presents a two-dimensional framework of separation between the correlation points and physical position from the TNTI to show interesting behaviour related to the location, size and intensity of velocity fluctuations with respect to the TNTI. We observe that the conditional velocity correlation functions exhibit distinct peaks at well-defined separations, indicating the typical scales of turbulent motions influenced by the TNTI. The values of the relevant peaks clearly demonstrate that, even when studied in a conditional framework, the dynamics of the velocity fluctuations with respect to for example the enstrophy, shows the presence of lengths scales that are very large with respect to the width of the turbulent region. Interesting results emerge when the correlation where one point is always fixed on the TNTI and the other interrogates the turbulent zone is considered . This observable investigates the turbulent dynamics inside the turbulent zone with respect to the TNTI. We show that the peak correlations are in line with the standard deviation of the TNTI, suggesting a connection to the scale of the turbulent motions attached to the TNTI. These features are not captured in classical statistics or in prior TNTI studies relying solely on one-point quantities.

I. INTRODUCTION

Turbulent flows generally consist of regions with different turbulence intensities. When considering a turbulent jet for example, turbulent fluctuations are released and evolve inside a (relatively) non-turbulent environment. Such non-turbulent environment may be completely free from turbulence or may be an environment having much lower turbulence

* Contact author: jean-paul.mollicone@um.edu.mt

intensity with respect to the turbulent jet.

The regions of high and low turbulence are separated by interfaces, or layers, across which important phenomena occur, such as momentum and energy transfer, which determine the growth and evolution of the flow, see da Silva *et al.* [1]. A specific interface between regions of high and low turbulence can be defined as the turbulent non-turbulent interface (TNTI). A common way to define the TNTI is by applying a threshold to a scalar field such as enstrophy, see Bisset *et al.* [2], Holzner *et al.* [3], da Silva and Pereira [4]. The interface is an artificial one since the transition from turbulent to non-turbulent fluid does not physically occur over a singular jump but must occur smoothly over a finite region. The threshold value is therefore taken in a range where the results conditioned on the TNTI are weakly sensitive to changes of the exact threshold value over that range, see Mathew and Basu [5], Westerweel *et al.* [6], Westerweel *et al.* [7]. The TNTI has been shown to be made up of two sublayers. One referred to as a viscous superlayer (VSL) where viscous effects dominate, first discussed many years ago by Corrsin and Kistler [8]. A second one referred to as a turbulent sublayer (TSL) or buffer layer where inertial effects dominate, see da Silva *et al.* [1], van Reeuwijk and Holzner [9], Borrell and Jiménez [10].

Analysing flow properties conditioned to the TNTI allows statistics to capture the intermittent nature of turbulent and non-turbulent flow regions defined by the TNTI. The TNTI shape is usually complex, owing to the turbulent structures in the flow, and therefore the flow properties change rapidly across the intricately folded interface. This conditional view differs from the classical averaged results where the flow properties are averaged over statistically homogeneous directions. The intermittent flow properties at the TNTI are therefore averaged out as the classical average combines statistics from both turbulent and non-turbulent regions.

Several studies use conditional averaging with respect to the TNTI to study a variety of phenomena related to the interface itself and the turbulence dynamics related to it. Westerweel *et al.* [7] analysed experimental data from turbulent round jets to study momentum and scalar transport phenomena at the TNTI. The entrainment dynamics at the TNTI were studied in detail using invariants of the velocity-gradient, rate-of-strain, and rate-of-rotation tensors by da Silva and Pereira [4]. van Reeuwijk and Holzner [9] performed a systematic study of the effect of the threshold value on the entrainment velocity and related statistics at the turbulence boundary of a temporal jet. A similar effect of conditional sampling and

its consequence on entrainment is studied for a turbulent plume by Burridge *et al.* [11]. Taveira and da Silva [12] investigated kinetic energy budgets near the TNTI in jets, which contributed to the understanding of energy distribution and dissipation at the interface.

Watanabe *et al.* [13] examined the scale-by-scale kinetic energy budget near the TNTI, detailing the energy dynamics across different scales whilst Silva *et al.* [14] show the scaling of the TNTI at high Reynolds numbers in the direct numerical simulations of temporal planar jets and shear free turbulence. From a Lagrangian point of view, Watanabe *et al.* [15] discuss entrainment properties relating to the VSL and TSL in direct numerical simulations of turbulent planar jets and mixing layers. Zecchetto and da Silva [16] show the universality of small-scale motions within the TNTI. van Reeuwijk *et al.* [17] derive an integral description of free shear flows capable of representing both the local and global viewpoints of turbulent entrainment. Studies related to the TNTI in boundary layers include the works by Ishihara *et al.* [18] that analysed conditional statistics near the TNTI of turbulent boundary layers, emphasizing the importance of conditional data in understanding turbulence and by Philip *et al.* [19] that conducted a multiscale analysis of fluxes at the TNTI in high Reynolds number boundary layers, offering a comprehensive view of flux interactions across scales.

Ishihara *et al.* [20] examined high Reynolds number turbulence using DNS results, highlighting the critical role of thin shear layers whilst Watanabe *et al.* [21] focused on enstrophy and passive scalar transport near the TNTI in a turbulent planar jet flow, providing insights into scalar dynamics at the interface. Both studies made valuable use of conditional statistics relative to interfaces, but in different flow contexts. Ishihara *et al.* [20] examined thin internal shear layers arising spontaneously in homogeneous isotropic turbulence within a periodic domain, and focused on one-point statistics across these high-vorticity zones, whilst on the other hand, Watanabe *et al.* [21] studied a spatially developing planar jet conditioning. The latter study focuses on one-point statistics of enstrophy and passive scalar fields on the distance from the turbulent/non-turbulent interface (TNTI), with further subdivision of the interface into leading, trailing, and side segments. Ishihara *et al.* [20] include scalar autocorrelation of velocity fluctuations in a part of their study but the definition of their interface is based on the thin shear layers in flow which is homogeneous turbulence, which is different from the TNTI we define in our work.

Our study involves a DNS of a temporal planar jet, which evolves homogeneously in time rather than space, and focuses on two-point velocity fluctuation correlations conditioned

(using two different approaches) on the distance from the TNTI (defined through an enstrophy threshold), together with showing the scaling characteristics of the statistics in time. While many studies have significantly advanced the understanding of conditional statistics near the TNTI, they predominantly focus on single-point statistics or flux analyses. The present work differentiates itself by employing two-point velocity fluctuation correlations to identify and characterise interesting behaviour related to turbulence dynamics at different scales in a planar temporal turbulent jet. The aims of this paper are as follows:

- To analyse one-point and two-point statistics of a Direct Numerical Simulation (DNS) of a planar turbulent temporal jet. The simulation uses a very extended domain to minimise artificial confinement of the growing jet, sufficient resolution to capture the TNTI dynamics accurately and a long evolution time.

- To compare statistics taken with respect to a spatially averaged turbulent non-turbulent interface (TNTI) to statistics taken conditionally to the instantaneous TNTI. The conditional statistics are of two types: one by considering statistics perpendicular to the streamwise direction and one by considering statistics normal to the TNTI.

- To demonstrate the self-similar scaling of one-point and two-point turbulence statistics over time, normalising these by a characteristic jet width derived from integral measures of volume and momentum fluxes. This will also validate the one-point correlations, serving as a methodological check against the more complex two-point correlations.

- To show that the standard deviation of the TNTI is seen as a recurrent value in results. For example, a significant difference in statistics between classical and conditional averages is seen at the TNTI and over a distance comparable to the standard deviation of the TNTI.

- To utilise two-point correlations of velocity fluctuations to identify and characterise interesting behaviour related to turbulence dynamics at various scales within the temporal jet.

- To investigate the scale of the turbulent structures that are inside the turbulent zone

but also attached to the TNTI. This is done by considering velocity fluctuation correlations where one point is anchored to the TNTI and the other extends into the turbulent region.

II. CASE SETUP

A temporal planar jet simulation [22, 23] is carried out by solving the incompressible Navier-Stokes equations,

$$\frac{\partial u_i}{\partial t} + \frac{\partial u_i u_j}{\partial x_j} = -\frac{1}{\rho}\frac{\partial p}{\partial x_i} + \nu \frac{\partial^2 u_i}{\partial x_j \partial x_j}, \quad \frac{\partial u_i}{\partial x_i} = 0, \tag{1}$$

where u_i are the velocity components, x_i are the geometrical directions (variables), ρ is the density and ν is the kinematic viscosity. Index $i = 1, 2, 3$ represents the streamwise, spanwise and vertical directions respectively with corresponding direction and velocity components referred to as (u, v, w) and (x, y, z) in the paper. The numerical code used is based on a fourth-order-accurate spatial discretization and a third-order Adams-Bashforth scheme for time integration, see Craske and van Reeuwijk [24]. The initial condition at time $t = 0$ is a fluid layer that is quiescent except for a thin region $-H < z < H$ where the streamwise velocity is non-zero and homogeneously distributed in the streamwise and spanwise directions,

$$u(x, y, z, 0) = \frac{U_0}{2}\left[1 + \tanh\left(\frac{H - |z|}{2\gamma_0}\right)\right] \tag{2}$$

where $\gamma_0 = 2H/35$ is the initial momentum thickness. An initial uniform random noise is superimposed with an intensity of 4% of the maximum initial velocity. The initial flow Reynolds number is $Re = U_0 H/\nu = 1000$ and the computational domain is a cuboid of size $L_x \times L_y \times L_z = 96H \times 96H \times 48H$ and has been discretized by using $2304 \times 2304 \times 960$ cells. Unless otherwise stated, variables are presented dimensionless by using H for lengths and H/U_0 for times. The flow in the simulation time $0 < t < 140$ decays and approaches a self-similar regime after an initial transition to turbulence [25, 26]. In this regime, a constant Taylor Reynolds number $Re_\lambda = \sqrt{2k_{cl}/3}\lambda_{cl}/\nu = 50$ is achieved where k_{cl} is the centerline turbulent kinetic energy and $\lambda = \sqrt{10\nu k_{cl}/\epsilon_{cl}}$ is the Taylor microscale with ϵ_{cl} the centreline turbulent dissipation. The total integration time for the simulation is $t = 160$. The domain is large compared to similar simulations by van Reeuwijk and Holzner [9] and da Silva and Pereira [4], therefore improving statistical convergence, but nonetheless retains a high grid

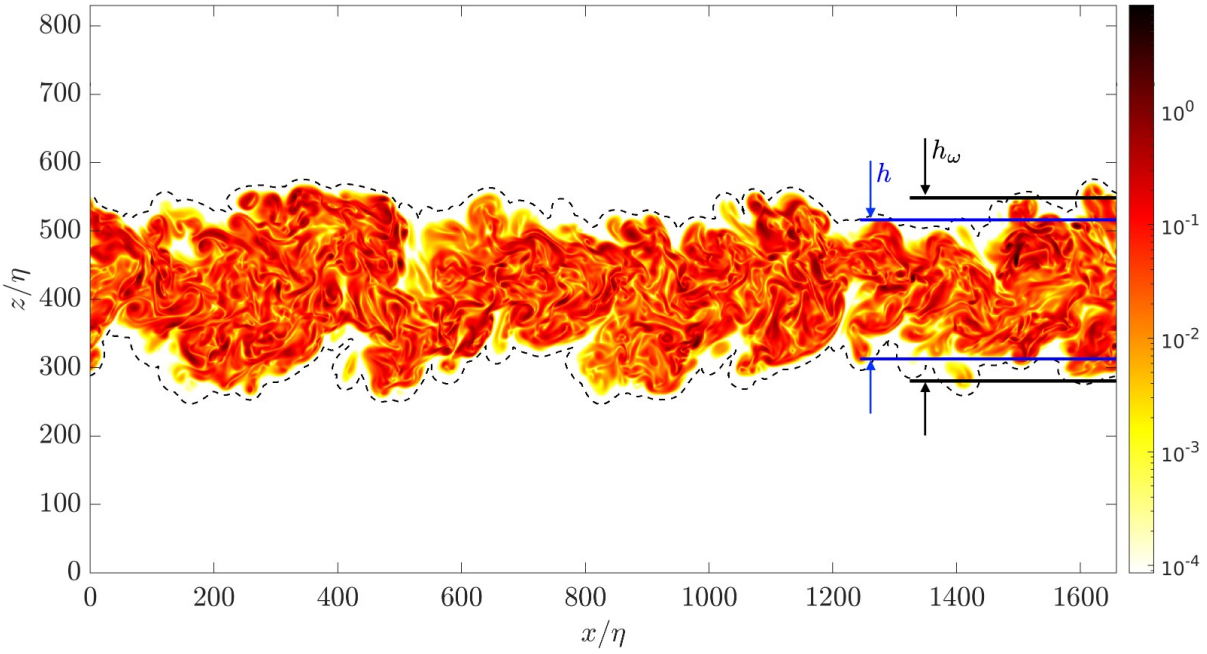

FIG. 1. Instantaneous two-dimensional plane of enstrophy $\omega^2 = \omega_i\omega_i$ with superimposed dashed black line representing the turbulent/non-turbulent interface (TNTI) defined with enstrophy threshold $\omega^2 = 1 \times 10^{-9}$ at time $t = 140$. Contour is in log scale and axes are normalised with the Kolmogorov scale η. The solid blue lines represent the vertical limits of the characteristic jet width h whilst the solid black lines represent the averaged (over the homogeneous directions x and y) interface height h_ω.

resolution with $\Delta x/\eta = \Delta y/\eta \approx 1.66$ and $\Delta z/\eta \approx 2$ at $t = 40$ where $\eta = (\nu^3/\epsilon_{cl})^{1/4}$ is the centerline Kolmogorov length scale. The Kolmogorov scale increases with time as $\sqrt{t}$ and with vertical position z, therefore improving the grid resolution. For more details on the flow and the quality of the simulation see Cimarelli *et al.* [22].

Figure 1 shows a two-dimensional slice of the instantaneous enstrophy $\omega^2 = \omega_i\omega_i$, where ω_i is the vorticity, at $t = 140$. The coordinate axes are normalised with the Kolmogorov length to emphasise the large domain used. The dashed line is the turbulent/non-turbulent interface (TNTI) defined as the iso-surface with constant enstrophy threshold $\omega^2 = 1 \times 10^{-9}$. Note that TNTI location variation is negligible for thresholds of order up to $\omega^2 \approx 1 \times 10^{-6}$. Let us highlight that this value is of the order of magnitude of the ones used in Holzner *et al.* [3] and quite smaller than that reported in Taveira and da Silva [12].

The enstrophy experiences a sudden drop in magnitude as it reaches the TNTI which

contains the turbulent part of the jet, as shown later in figure 4 in section III. The blue lines in figure 1 represent the vertical limits of the characteristic jet width h. The volume flux Q and the momentum flux M can be used to define h and the characteristic jet velocity u_h, where

$$Q = \int_0^\infty \langle u \rangle_{NC} \, dz, \quad M = \int_0^\infty \langle u \rangle_{NC}^2 \, dz, \quad h = \frac{Q^2}{M}, \quad u_h = \frac{M}{Q}, \tag{3}$$

where the brackets $\langle \rangle_{NC}$ represent the non-conditional (classical) average in the homogeneous directions x and y. The height h and velocity u_h are used to normalise the results in section III. The black lines in figure 1 represent on the other hand h_ω, that is the width defined by TNTI location integrated over the turbulent volume V_T

$$h_\omega = \frac{1}{L_x L_y} \iiint_{V_T} dV. \tag{4}$$

Note that V_T is limited by the (instantaneous) surface of the TNTI, Ω_T, and the four planes where the periodic boundary conditions are applied. In the self-similar regime, the characteristic jet width scales linearly with the integral interface height, $h \sim h_\omega$, see van Reeuwijk and Holzner [9]. The proportion constant is $a_\omega = 0.75$ when calculated from $h = a_\omega h_\omega$ for simulation times $100 < t < 140$. It is worth mentioning that the value of $h_\omega/2$, that is inherently a conditional quantity, is much smaller than the value h_Ω that can be defined based on the average value of the non-conditional enstrophy budget, see e.g. Cimarelli *et al.* [22].

Figure 2 shows the three types of averaging used to calculate TNTI statistics (left to right), each described for one-point (top panels) and two-point (bottom panels) correlations, taking the velocity fluctuation u' as an example. The three types of averages for a generic variable χ are defined as

$$\langle \chi \rangle_{NC}(d) = \frac{\int_{\overline{\Omega}_T} \chi(\mathbf{x} + \overline{\mathbf{n}} d) \mathrm{d}S}{\int_{\overline{\Omega}_T} \mathrm{d}S}, \tag{5}$$

$$\langle \chi \rangle_{CV}(d) = \frac{\int_{\Omega_T} \chi(\mathbf{x} + \frac{\mathbf{n}\cdot\mathbf{k}}{|\mathbf{n}\cdot\mathbf{k}|} d) \mathrm{d}S}{\int_{\Omega_T} \mathrm{d}S}, \tag{6}$$

$$\langle \chi \rangle_{CN}(d) = \frac{\int_{\Omega_T} \chi(\mathbf{x} + \mathbf{n} d) \mathrm{d}S}{\int_{\Omega_T} \mathrm{d}S}, \tag{7}$$

where $\mathbf{x}$ is the instantaneous TNTI position vector, $\mathbf{n} = \nabla\omega^2/|\nabla\omega^2|$ is the normal to the instantaneous TNTI (positive pointing into the turbulent zone), $\overline{\mathbf{n}}$ is the normal to the average TNTI position (h_ω), $\mathbf{k}$ is the unit vector in the z (vertical) direction and $\overline{\Omega}_T$ is the

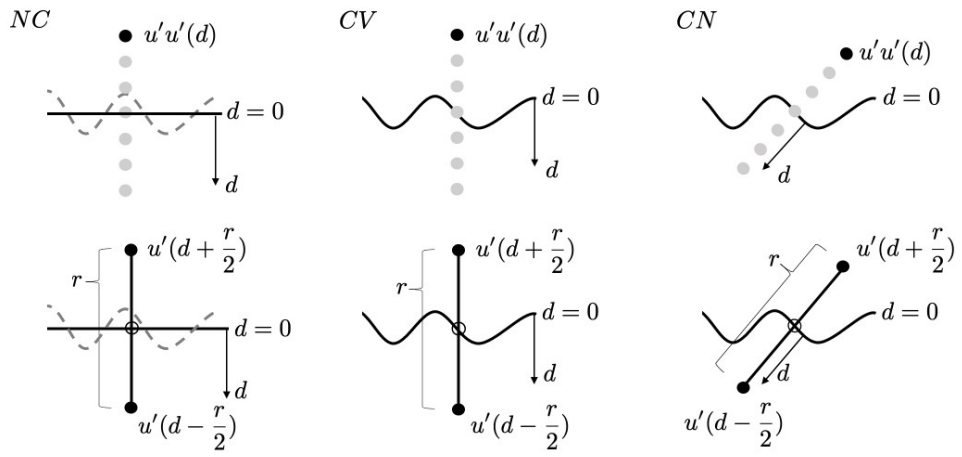

FIG. 2. The different types of averaging considered (left to right) for one-point and two-point statistics (top and bottom, respectively). NC: Averaging taken with respect to mean interface height h_ω. CV: conditional averaging with respect to local interface location with separation vector r parallel to the z direction. CN: same as CV except that separation vector r is taken normal to the interface.

averaged TNTI position defined by h_ω. For the conditional normal averaging (CN) it is worth pointing out that we use the procedure of Taveira and da Silva [12], i.e. each (x, z) plane is treated independently and hence we consider the normal vector calculated in that plane.

For all the type of averaging defined in equations (5, 6, 7) a decomposition of the flow, $u_i = \langle u_i \rangle + u_i'$, is applied to calculate the velocity fluctuation fields u_i' relative to the three mean velocities $\langle u_i \rangle$. The TNTI location reference is taken at $d = 0$ and $d > 0$ is taken in the direction of the jet core in the turbulent zone. The non-conditional (NC) average is performed with respect to the spatially averaged TNTI location, represented by the solid line in figure 1 and figure 2(NC). The dashed curves in figure 1 and the NC sketches in figure 2 represent the instantaneous TNTI. The other two types of averaging, CV and CN, are taken conditional to the instantaneous TNTI location (solid black line). CV is always represented as a function of the vertical distance from the TNTI whilst CN is represented as a function of the normal distance to the TNTI.

The top sketches in figure 2 show the one-point correlation $u'u'(d)$ which is only a function of the distance from the interface d. The bottom sketches show the two points used for

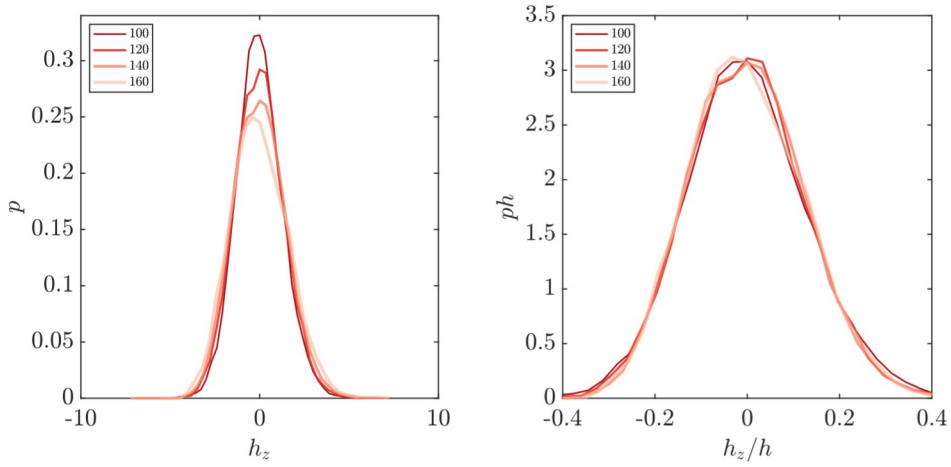

FIG. 3. TNTI probability density function (PDF) at $t = [100, 120, 140, 160]$ in the left panel and the corresponding plots with the probability p against the distance $h_z(x, y, t)$ of the TNTI from its average position normalised using the characteristic jet width h in the right panel.

the multi-scale correlations $u'(d + r/2)u'(d - r/2)$ which are a function of both d and the separation vector r. In this case d represents the distance from the TNTI to the mid-point of the separation between the two points. The complexity and time required in calculating the correlations increases from NC to CV to CN and also from the one-point to the two-point statistics. Statistics are averaged in the homogeneous streamwise x and spanwise y directions. For the sake of simplicity in the figures, the averaging is denoted by the brackets $\langle\,\rangle$ and the type of average represented will be described in the legend. Since the flow is symmetrical in the vertical direction z about the centerline $z = 0$, the top and bottom halves are also averaged to enhance statistical convergence. The data are not averaged in time since the jet evolves temporally. If the TNTI is intersected more than once along the sampling directions, statistics are discarded. The probability of this occurring is low and only a small portion of statistics are discarded.

III. RESULTS

As a first validation of the very large data set available, in this section we present some preliminary statistics of the temporal jet that are based on the enstrophy field. We stress that due to the statistical convergence we are able to test the time behaviour of most of the

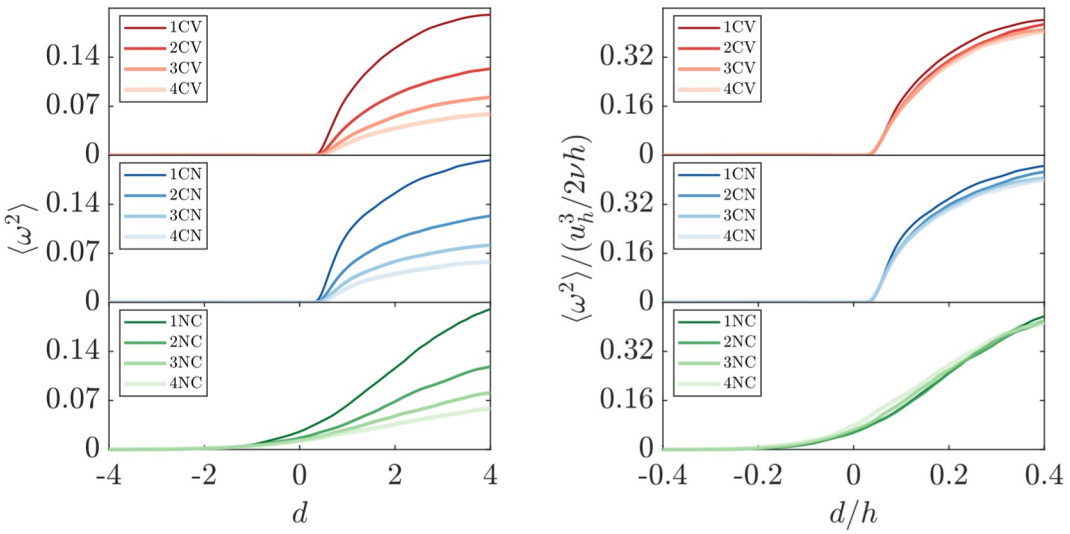

FIG. 4. Enstrophy $\langle\omega^2\rangle$ (left panel) and enstrophy normalised with $(u_h^3/2\nu h)$ (right panel) as a function of distance from the interface at $t = [100, 120, 140, 160]$ averaged using NC, CV and CN types of averaging.

observables that we discuss in the remainder of the paper.

In the left panel of figure 3, the probability density function (PDF) of the distance $h_z = h_z(x, y, t)$ of the TNTI from its average position $h_\omega = h_\omega(t)$ is shown for times $t = [100, 120, 140, 160]$. The different shades of colour represent the different times. The right panel shows the same plots but with the probability p and h_z normalised using the characteristic jet width h. The plots collapse onto each other showing self-similarity in time. A Gaussian distribution, defined as $P(h_z) = \frac{1}{\sigma\sqrt{2\pi}} e^{-{h_z}^2/2(\sigma)^2}$, fits onto the PDF in the right panel of figure 3 and the standard deviation was found to be $\sigma = 0.13h$.

The left panel of figure 4 shows the mean enstrophy $\langle\omega^2\rangle$ as a function of distance d from the interface at $t = [100, 120, 140, 160]$. Different colour shades represent the different times. CV, CN and NC are shown in red, blue and green from top to bottom panels respectively. For the conditional averaging cases CV and CN, the enstrophy increases rapidly as the TNTI is crossed from the non-turbulent zone into the turbulent zone, that is as d becomes positive, in agreement with literature such as similar conditional enstrophy plots by Watanabe *et al.* [21]. For the sake of clarity, figure 5 also shows the points where the statistics are evaluated when we consider CV, in particular the black line is the section of the surface where the statistics at $d/h = 0.5$ are calculated. On the other hand, the increase is smooth for the

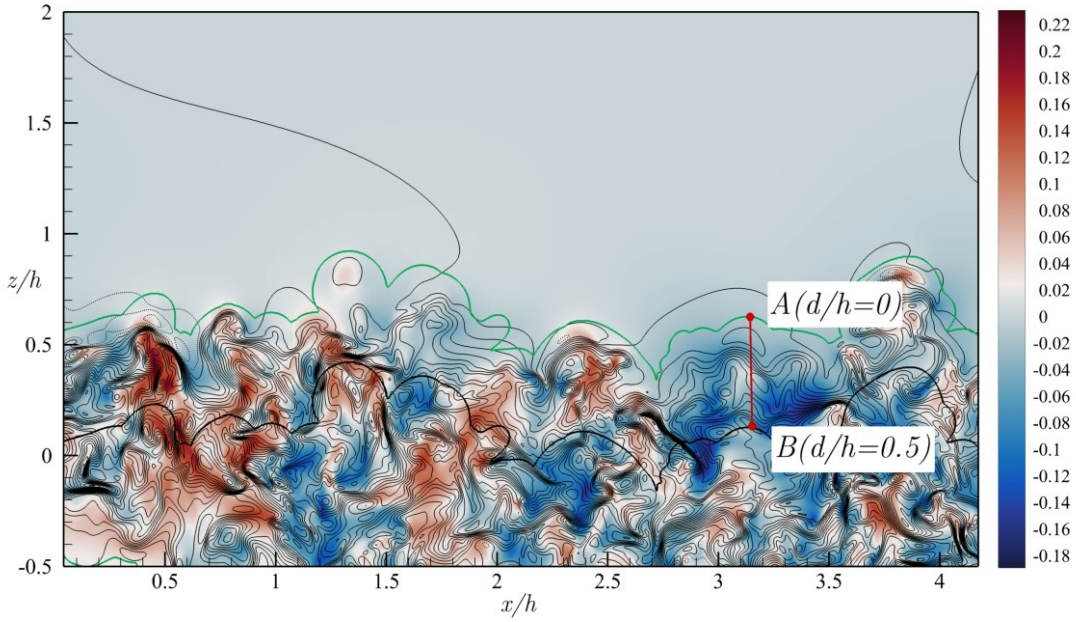

FIG. 5. Instantaneous two-dimensional plane of two components of the velocity: u represented with lines and w represented with colour at time $t = 140$. The solid green line represents the position of the interface at $\omega^2 = 1 \times 10^{-9}$ while the thicker black line represents $d/h = 0.5$ for the CV statistics.

NC case and there is no clear sign of the presence of the TNTI, even though an averaged TNTI height is used as reference at $d = 0$. The right panel shows the equivalent plots but with the enstrophy normalised by $(u_h^3/2\nu h)$, following from the definition of turbulent dissipation $\epsilon = 2\nu\omega^2$ (from an isotropic picture of turbulence), and the distance normalised using the characteristic jet width h. The plots now clearly collapse onto each other showing self-similarity in time. The plots would still collapse using u_h^2/h^2, as sometimes used in the literature, however this would not work for other flows, for example at different Reynolds numbers, since enstrophy is fundamentally a small-scale property.

A. Mean velocities

The conditional mean streamwise $\langle u \rangle$ and normal velocity $\langle w \rangle$ profiles for four different times are displayed in the left and middle plots of figure 6, respectively. Due to the statistical symmetries of the flow the value of $\langle v \rangle$ is zero for the three type of statistics. The conditional averaged streamwise velocity appears to be different from the classical one, reported in the plot only for the case at $t = 140$. The conditional curves show an excellent scaling behaviour in time for both components of the velocity. The value of the streamwise component is constant in the irrotational region and increases sharply near the TNTI. The steep gradient observed in the conditional mean velocity across the TNTI is indicative of the strong shear layer that marks the interface. This steepness is directly tied to the presence of entrainment-generated vorticity and is consistent with prior observations of TNTI sharpness in jets and boundary layers. The thickness over which this gradient develops corresponds well with the standard deviation of the TNTI location, reinforcing the idea that turbulent influence extends only a short distance into the non-turbulent region.

When comparing our data with the same observable shown in [12] we can notice that the value of the mean velocity in the non-turbulent region is very low for our dataset. We argue that this difference can be attributed to the much lower values of enstrophy that we choose to separate the turbulent and non-turbulent parts of the flow which moves the interface farther away from the center of the jet. Addressing the middle plot of figure 6, we observe that the conditional normal velocity $\langle w \rangle$ is negative in the irrotational flow and is positive in the turbulent region. Considering the top interface of figure 1, in such a case, $\langle w \rangle < 0$ in the irrotational region is related to a transport of fluid toward the center of the jet while $\langle w \rangle > 0$ in the rotational part is related to the expansion of the turbulent jet. To justify this behavior we can start by considering that in the case of the NC statistics taken at any the horizontal surface at a distance d from $\overline{\Omega}_T$ defines the boundary of control volume through which the mass flux, represented by $\langle w \rangle$, has to be zero. This is not true anymore for the corrugated interface where the flux is also controlled by the other velocity components. In fact, when considering the control volume V_T, remembering that the surface integrals on the periodic boundaries of the computational domain cancel out, for a divergence free velocity field we can write

$$\iiint_{V_T} \nabla \cdot \mathbf{u} \, dV = \iint_{\Omega_T} \mathbf{u} \cdot \mathbf{n} \; \mathrm{d}S = 0 \tag{8}$$

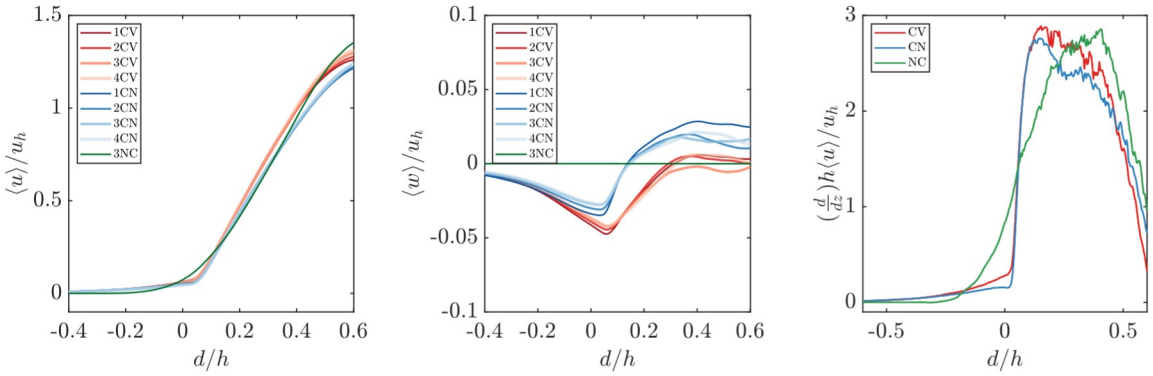

FIG. 6. From left to right: average velocities $\langle u \rangle$ and $\langle w \rangle$ and derivative of u $\langle u \rangle$ normalised with u_h as a function of distance d/h from the interface. Positive d indicates the turbulent zone towards the centre of the jet. CV, CN and NC represent vertical conditional, normal conditional and non-conditional averaging, in dark, light and dashed lines, respectively. The last plot shows the three derivatives at $t = 140$.

where the scalar product in the surface integral can be written as $\mathbf{u} \cdot \mathbf{n} = un_x + vn_y + wn_z$. Hence, from the last equality of equation 8 we obtain

$$\langle w \rangle = \frac{1}{\iint_{\Omega_T} \mathrm{d}S} \iint_{\Omega_T} wn_z \, \mathrm{d}S = -\frac{1}{\iint_{\Omega_T} \mathrm{d}S} \iint_{\Omega_T} (un_x + vn_y) \, \mathrm{d}S \tag{9}$$

where the average is obtained by dividing by the surface area of Ω_T. From equation (9) we can observe that the conditional mean value of the vertical velocity is related to the geometrical redistribution of the velocity and the normal to the interface.

When comparing the two conditional statistics we realise that the CV recovers the zero value of the NC in the turbulent region possibly implying that further away in the turbulent region the points sampled by the vertical conditional statistics do not feel the signature of the interface and recover the non-conditional ones. Note that the values at $d/h = 0$ are slightly different for the two statistical approaches (CV or CN) when these should be equal given that, on the TNTI and for $r/h = 0$, the sampling direction should have no effect. We attribute this slight difference due to some statistics being discarded if the TNTI is intersected more than once along the sampling directions, as already mentioned. Even though the probability is low and only a few data are discarded, this can slightly skew the statistical average.

The right plot of figure 6 shows the derivative of $\langle u \rangle$ with respect to the distance from

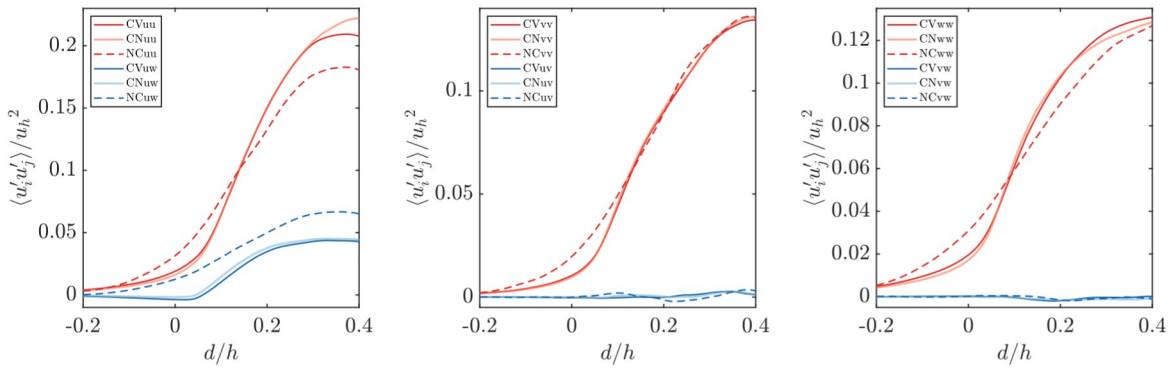

FIG. 7. Reynolds stresses $\langle u_i' u_j' \rangle$ (see legend) normalised with u_h^2 as a function of distance d/h from the interface for separation vector $r/h = 0.0$ at time $t = 140$. Positive d indicates the turbulent zone towards the centre of the jet. CV, CN and NC represent vertical conditional, normal conditional and non-conditional averaging, in dark, light and dashed lines, respectively.

the interface at $t = 140$. This plot clearly quantifies the sharper rise of the conditional velocity. The overall behavior of the derivative is very similar to that found in a round jet by Westerweel *et al.* [7]. The sharp features visible in the conditional correlations, in contrast to the smoother trends in the classical statistics, emphasise the importance of aligning the analysis with the TNTI. Classical averaging smears over spatial variability in interface location and thereby underestimates the true spatial coherence of turbulence dynamics near the interface. This highlights the TNTI as an organisational feature in the flow, rather than just a statistical threshold.

B. Reynolds-Stress Tensor

The Reynolds-stress tensor components are analysed separately to observe behaviour across the turbulent non-turbulent interface (TNTI) and towards the jet core when the different types of averaging are used. We would like to stress that, as mentioned in the previous section, the velocity components are decomposed in different ways for the three different statistical approaches accordingly to the three definitions of the mean. Figure 7 shows the Reynolds stresses $\langle u_i' u_j' \rangle$ normalised with u_h^2 as a function of distance d/h from the interface at time $t = 140$. The TNTI is located at $d = 0$ and $d > 0$ indicates the turbulent zone (towards the jet core) whilst $d < 0$ indicates the non-turbulent zone. CV, CN and

NC represent the different types of averaging, as discussed in section II, in dark, light and dashed lines, respectively. The tensor components and their respective colour for each plot are indicated in the legend. In this section the discussion will focus mostly on the dynamics across the interface and the comparison between the various averaging approaches. The behaviour at large values of d will be discussed in more detail in the next section. From left to right, the plots show the three trace components, $\langle u'u' \rangle$, $\langle v'v' \rangle$ and $\langle w'w' \rangle$, in red in all panels, together with $\langle u'w' \rangle$, in blue in the left panel. The remaining components, $\langle u'v' \rangle$ and $\langle v'w' \rangle$, are zero throughout and are therefore not discussed even if they are reported in the middle and right panel. The only non-zero mean turbulent shear stress occurs in the x-z plane and all the trace components contribute to the turbulent kinetic energy.

The superposition of CV and CN (solid lines) shows that the difference between taking the conditional average in the vertical direction (CV) or normal to the TNTI (CN) is negligible. The similarity observed between the CV and CN conditional statistics in our results holds specifically for the large-scale quantities analysed here, such as Reynolds stresses and two-point velocity fluctuation correlations. For small-scale quantities the CV and CN approaches can yield notably different results due to the high sensitivity of such quantities to orientation and local curvature of the TNTI, see Watanabe *et al.* [27]. In the present statistics, we focus on velocity fluctuations and their spatial correlations over scales of the order of the TNTI deviation and the jet half-width. In this case, CV and CN yield nearly identical results, suggesting that for these large-scale, low-order statistics, vertical conditioning (CV) is a good approximation to the more complex interface-normal (CN) approach. This has significant implications on the complexity and time required to calculate correlations since CV averaging is relatively simpler to implement and faster to compute. When dealing with large data sets and higher order statistics, the time needed for CN averaging can be orders of magnitude higher than CV averaging. The highest computational cost for the post-processing of CN averaging comes from the need to find the normal at each point along the TNTI and then interpolating all the values required along the normal since they will practically never coincide with values at the grid nodes.

We decide to start the detailed discussion of the results from the middle plot of figure 7 where the profile of $\langle v'v' \rangle$ is shown. It is worth underlining that for this observable the differences between the classical and conditional averages are only due to the statistical ensemble where the average is taken as the values of the fluctuations are the same for all the

three approaches being $\langle v \rangle = 0$. In this case the three types of averaging coincide with each other except for the region close to the TNTI. On the other hand for the other components of the Reynolds stress tensor, NC averaging (dashed lines) also departs from CV and CN in various locations.

Similarly to the mean profile discussed in the previous subsection, CV and CN correlations show a jump when crossing the TNTI into the turbulent zone, see Westerweel *et al.* [7], while NC increases in magnitude with a smoother slope towards the peak values at the jet centre. A significant difference, well above 50%, is always present at the interface location for all the tensor components. Based on the observation reported previously on the $\langle v'v' \rangle$ plot we argue that this difference across $d/h = 0$ can be mostly attributed to the TNTI deviation from its average location as shown by the probability density function (PDF) in figure 3. NC is taken with respect to the averaged interface height that intersects the convoluted TNTI horizontally. Unlike CV/CN, NC does not shift with the TNTI location and averages variables indiscriminately over turbulent and non-turbulent regions since it uses the single averaged interface height as the TNTI location reference at $d = 0$. A significant difference is present even though the choice of a low enstrophy threshold results in a relatively smooth TNTI. The PDF's standard deviation $\sigma = 0.13h$ corresponds to the distance from $d/h = 0$ that marks the region where NC and CV/CN plots do not coincide, that is where they diverge at $d/h \approx -0.15$ and where they converge again at $d/h \approx +0.15$, see the plots in figure 7. Differences between NC and CV/CN are also present further into the turbulent region for $\langle w'w' \rangle$ and $\langle u'u' \rangle$ at $d/h \approx 0.1 - 0.3$ and $d/h \gtrsim 0.2$ respectively. It is clear that the differences that we observe towards the center of the jet could be attributed not only to the different sets of points where the statistics is calculated but also to the changes of the fluctuation value.

The shear stress component $\langle u'w' \rangle$ is persistently different throughout, from the TNTI region to the jet core. It is well established that turbulence entrains irrotational fluid from the surrounding non-turbulent region, generating complex velocity fluctuations. While such entrainment dynamics are known, our analysis focuses specifically on how these interactions manifest in the behavior of the Reynolds shear stress $\langle u'w' \rangle$.

At the TNTI, CV/CN shows negative values and becomes positive only inside the turbulent region whilst NC gives a steadily increasing positive value as it crosses the TNTI. In the classical average, the sign of the shear stress component is generally attributed to the

sign of the fluctuations due to the turbulent motions. As shown in Cimarelli *et al.* [23], in most of the turbulent region near the TNTI we observe the presence of quasi-streamwise vortices. The presence of these vortices coupled with the mean velocity can easily explain the positive sign of $\langle u'w' \rangle$ in the NC average. On the other hand, in the conditional average context, the result has a slightly more complex interpretation. It is possible to argue that the observed behaviour is due to the fact that, in the conditional statistics, we clearly separate the average dynamics of the irrotational velocity fluctuations from the rotational ones. In other words, the statistics observed in figure 7 very close to the putative position of the interface is obtained completely screening the rotational fluctuations and we argue that the negative values of the correlation we observe for $\langle u'w' \rangle$ are the signature of the irrotational fluctuations near the TNTI. It is worth repeating that due to the very low value of the enstrophy threshold chosen in this work we can assume that for values up to $d/h \approx 0.1$ we are sampling substantially irrotational regions.

Our conditional statistics (CV and CN) reveal that $\langle u'w' \rangle$ becomes negative in a narrow region near the TNTI, in contrast to the classical statistics where it remains positive. To explain this, when considering the fluctuations in the vicinity of the TNTI, fluid moving outward from the jet core ($w' > 0$) tends to have lower-than-average streamwise velocity ($u' < 0$), while fluid moving inward ($w' < 0$) tends to have higher-than-average u'. In both cases, u' and w' are anti-correlated, leading to $\langle u'w' \rangle < 0$. This represents a counter-gradient transport of momentum, which is distinct from the positive correlation typically observed in turbulent shear flows.

This finding can be linked to the turbulent kinetic energy (TKE) budget, specifically the production term $-\langle u'w' \rangle \partial U/\partial z$ which represent the transfer from the the kinetic energy of the mean velocity field. In the near-TNTI region of the upper interface, the mean velocity gradient remains negative, as confirmed in both classical and conditional averages (see figure 6, right panel). However, due to the negative $\langle u'w' \rangle$, the TKE production term becomes negative, implying that energy is being transferred from the turbulent fluctuations back to the mean flow, a sign of turbulence suppression in the entrainment layer. This sign reversal has important implications for turbulence modeling. Conventional turbulence models, such as those based on the eddy viscosity concept, typically assume positive production. These models cannot reproduce the sign reversal we observe, which highlights a significant limitation in their application to TNTI regions. That is, interface-localized dynamics may not

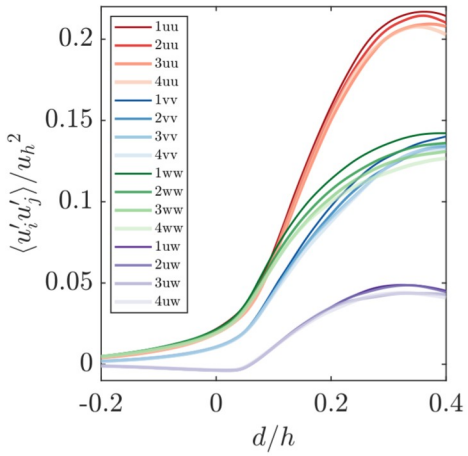

FIG. 8. Reynolds stresses tensor trace, $\langle u_i' u_i' \rangle$, and shear component $\langle u'w' \rangle$ (see legend) normalised with u_h^2 as a function of distance d/h from the interface for separation vector $r/h = 0.0$ at times $t = [100, 120, 140, 160]$ using CV. Different times are shown by varying the line style and are denoted by 1 to 4 in the legend respectively. Positive d indicates the turbulent zone towards the centre of the jet.

be adequately represented in classical closures and may require non-local or interface-aware modeling strategies.

After establishing that CV and CN differences are qualitatively negligible, we focus on the CV results for the rest of the paper. The scaling in time is now analysed. Figure 8 shows the three tensor trace components and shear component at times $t = [100, 120, 140, 160]$ using CV averaging. All components exhibit self-similarity in time as the plots collapse onto each other along all the distance d/h when normalised with u_h^2. The figure clearly shows the difference in magnitudes for the components. Component $\langle u'u' \rangle$ is the largest whilst $\langle v'v' \rangle$ and $\langle w'w' \rangle$ have similar magnitudes.

C. Two-Point Correlations

The analysis is now extended to two-point statistics, that is, when a separation exists ($r/h \neq 0$) between points that are used to calculate the multi-scale correlations. Two-point correlations of velocity fluctuations provide a fundamental tool for understanding the coherent structures present in turbulent flows [23]. They measure the degree to which

turbulent fluctuations at different points in the flow are related to each other. When these correlations are strong, it indicates a high level of coherence between the turbulent fluid motions at these points, which is a signature of large-scale organized structures such as vortices or eddies.

In this section we will analyse the correlation between points that are conditionally positioned with respect to the TNTI. Given a point at a fixed distance d from the interface, as sketched in figure 2, the first and second points are located at two physical positions which are at distances $r/2$. We show here only results obtained via the CV average where the separation vector r is always parallel to the z direction. The complete picture, at a glance, can now be discussed by looking at the whole two-dimensional correlation space for a fixed time presented in figure 9. In the plot, the two-point correlations are shown as a function of the normalized separation (r/h) and normalized physical position (d/h) and hence the effect of velocity structures conditional to the TNTI can be investigated.

The black dashed line represents $d = |r/2|$, below which any correlation consists of two points that are always inside the putative turbulent zone defined by the chosen threshold. In particular, moving along that line we consider the correlation between points where one is always positioned on the interface. Note that the jet centreline coincides with $d/h \approx 0.67$, hence we are looking at very large scale structures. The top panels show the auto correlations for the velocity components whilst the bottom panel shows the correlation for $\langle u'w' \rangle$. Note that the correlation that we will refer to as $\langle w'u' \rangle$ is incorporated in the plot of $\langle u'w' \rangle$ for values $r/h < 0$. Consequently, $\langle u'w' \rangle = \langle w'u' \rangle$ for $r/h = 0$, which represents the one-point correlations.

The two-dimensional space allows us to clearly identify correlation peaks and their shapes across both distance and separations. We will start addressing the behaviour at $r/h = 0$ which are exactly the same plots discussed in the previous section. The positive peaks are centered at $d/h \approx 0.35$ for all the plots reported in Figure 9. The existence of a peak is normally an indication of the existence of vortical structures centered at its location. Indeed, when rescaling the position of the peak with respect to h_ω we see that the peak is approximately midway between the edge of the rotational region and the center of the jet i.e. $d/h_\omega \approx 0.27$. These very large scales characterizing the dynamics of the velocity fluctuations are in agreement with the conditional analysis already performed on this dataset within the

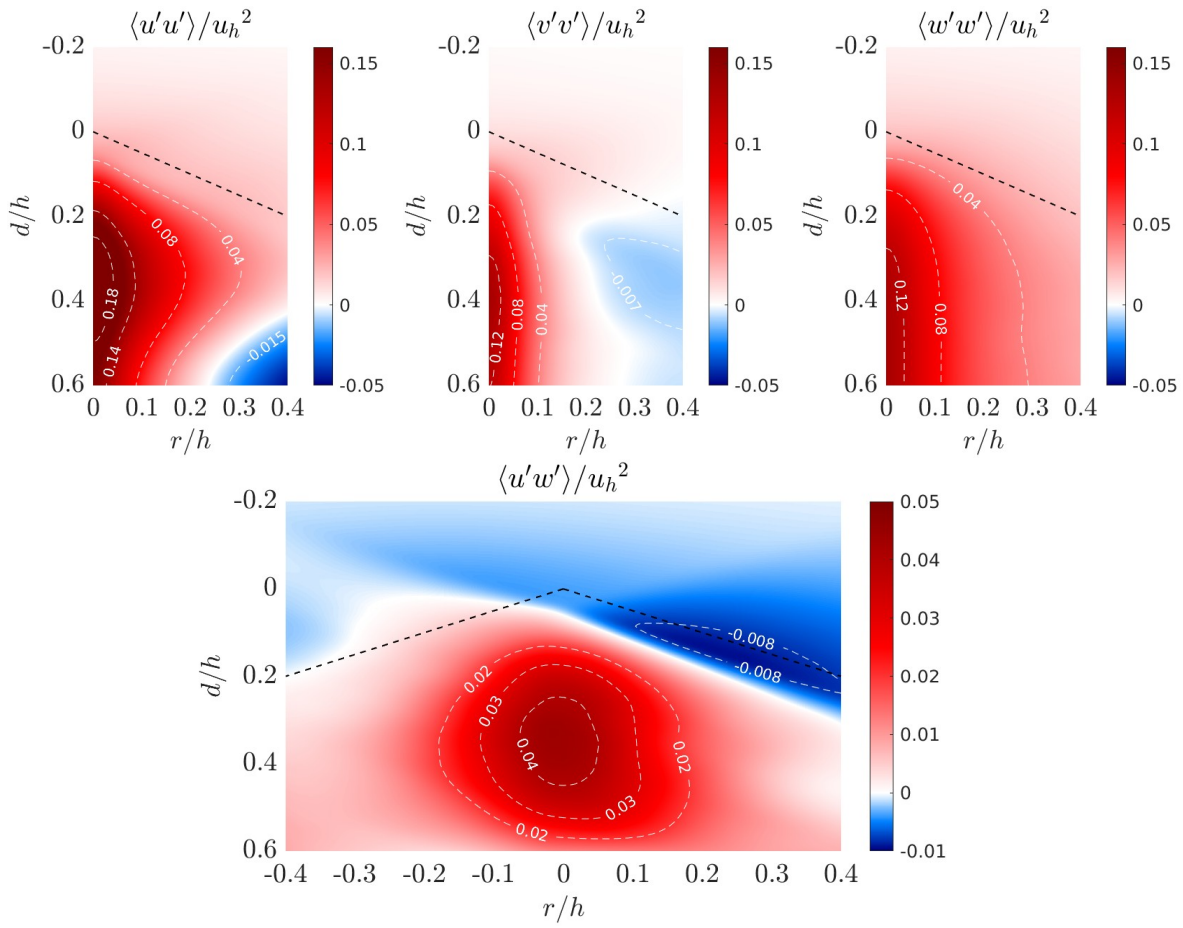

FIG. 9. Two-point correlations in the two-dimensional space of distance (d/h) from the TNTI against separation (r/h) at time $t = 140$ using CV averaging. The black dashed line represents $d = |r/2|$.

classical statistical framework and presented in Cimarelli *et al.* [23].

To expand on the effect of the TNTI and to analyse the structures attached to it, figure 10 shows plots of correlations along the line $d = |r/2|$ (that is, along the black dashed lines in figure 9). Since d is the mid-point, for the correlation to follow $d = |r/2|$, the separation is such that one point is always fixed on the TNTI whilst the other point moves into the turbulent zone as r/h increases, see for clarity points A and B, respectively, in figure 5 where $r/h = 0.5$. The correlations on that line therefore interrogate turbulent structures inside the turbulent zone that are attached to the TNTI. In analysing the correlation along this line we argue that the behaviour we observe can be better understood considering that the fluctuations at the putative position of the interface are more consistent with an

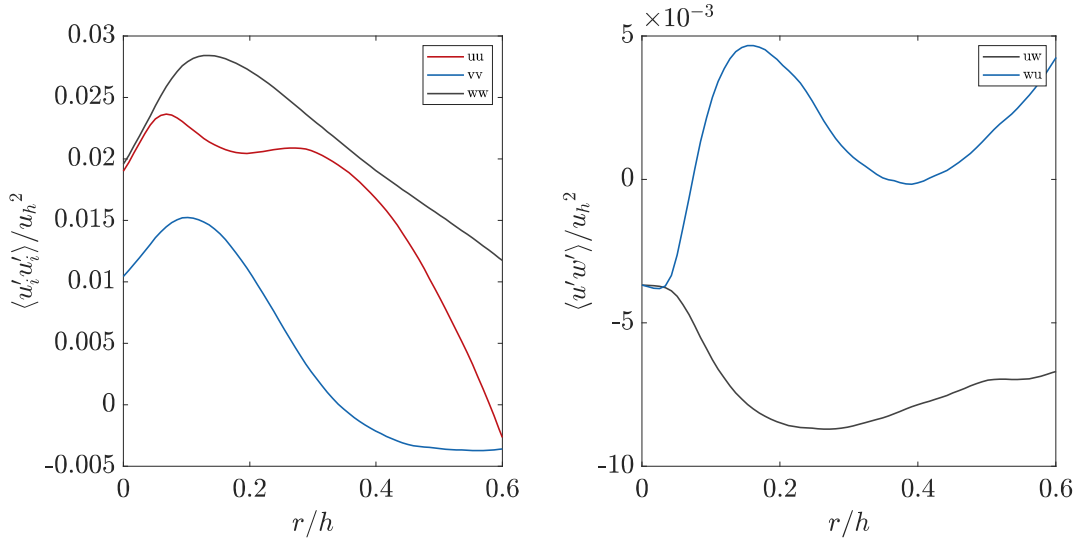

FIG. 10. Correlations along the line $d = |r/2|$ plotted as a function of separation r/h at time $t = 140$ using CV averaging.

irrotational velocity field. In detail, $\langle u'u' \rangle, \langle v'v' \rangle$ and $\langle w'w' \rangle$ exhibit a peak in the range of $r/h = 0.1 \pm 0.04$. We speculate that this larger value of the correlation is the signature of large fluctuations occurring at that distance from $d = 0$. This observation seems to suggest that the edge of the large scale velocity structures that we have identified above is positioned at this distance from the interface. The location of the peaks in figure 10 is in line with the interface PDF standard deviation and therefore suggests a connection with the scales of the structures attached to it. Moving to larger values of r/h, the decay in correlation as the separation increases is different for the three components and $\langle u'u' \rangle$ exhibits a secondary peak at $r/h \approx 0.3$. It is worth noting that for the $\langle u'u' \rangle$ and $\langle v'v' \rangle$ components, the correlation becomes negative for r/h of the order of the distance of the interface from center of the jet, thus indicating the presence of large vortical structures covering at least half of the width of the jet.

Returning to the analysis of figure 9, interesting features arise across the plots when considering the line below $d = |r/2|$. The peaks are contained beneath this line and their location is shifted and shaped by it. The correlation regions in its vicinity align with it such as, for example, the iso-contours $\langle u'u' \rangle = 0.04$, $\langle w'w' \rangle = 0.4$ or $\langle u'w' \rangle = -0.008$. In the latter case, the white contour colour separating positive and negative correlation regions is also aligned with $d = |r/2|$ for $r/h > 0$. The peak for $\langle u'u' \rangle$ extends to larger separations at

$d/h \approx 0.3$ and reduces as an anti-correlated region appears for larger separations towards the jet centreline. The $\langle v'v' \rangle$ peak is further contained at separations $r/h < 1.0$ and has an elongated shape extending towards the jet centreline as an anti-correlation region is present for larger separations across all the turbulent region. On the other hand, $\langle w'w' \rangle$ presents no anti-correlated regions and extends smoothly to all scales inside the turbulent zone. The positive peak for $\langle u'w' \rangle$ takes a circular form, centered at $r/h = 0$ and $d/h = 0.35$, and extends to both positive and negative separation values.

A significant anti-correlated peak that is aligned with $d = |r/2|$ spans across all separations when $r/h > 0$. The values of the relevant peaks clearly demonstrate that, even when studied in a conditional framework, the dynamics of the velocity fluctuations, with respect to for example enstrophy, shows the presence of lengths scales that are very large with respect to the width of the turbulent region. When considering negatively correlated regions, we recall the discussion in the previous section regarding their significance and their effect on the sign of the production term in the TKE equation. Here, in an analysis which is considering two-point correlations, the results show that such considerations now extend across a range of scales. As previously discussed, this has implications on turbulence modelling when using LES models based on subgrid viscosity.

The shear components $\langle u'w' \rangle$ and $\langle w'u' \rangle$ instead show contrasting behaviour on the attached line, see both figure 9 and figure 10. The former is always negatively correlated whilst the latter increases from an initial negative correlation to a positive correlation peak just below $r/h = 0.2$. In order to discuss this behaviour we must remember that for $\langle u'w' \rangle$ we consider a streamwise fluctuation at the interface and a vertical fluctuation inside the turbulent region, while the opposite is for $\langle w'u' \rangle$. Just limiting here our speculation at the former, this statistical observable seems to be compatible again with the existence of layer of a certain width where the behaviour of the fluctuations is irrotational. In particular this effect is observable when looking at statistics where the outermost point is within a layer of $\Delta d/h = 0.05$ from the putative interface. To strengthen these observations we can look at the $\langle u'u' \rangle$ and $\langle u'w' \rangle$ correlations in figure 11 that will be further discussed later in this section. From a quantitative point of view, we observe that the correlation between points such that $d - |r|/2 < 0.05h$ behaves linearly. As soon as the outermost point enters the fully turbulent region, the correlation starts increasing rapidly and in a non-linear way. The comparison of the two bottom plots in figure 11 suggest that this discontinuity in the statistical

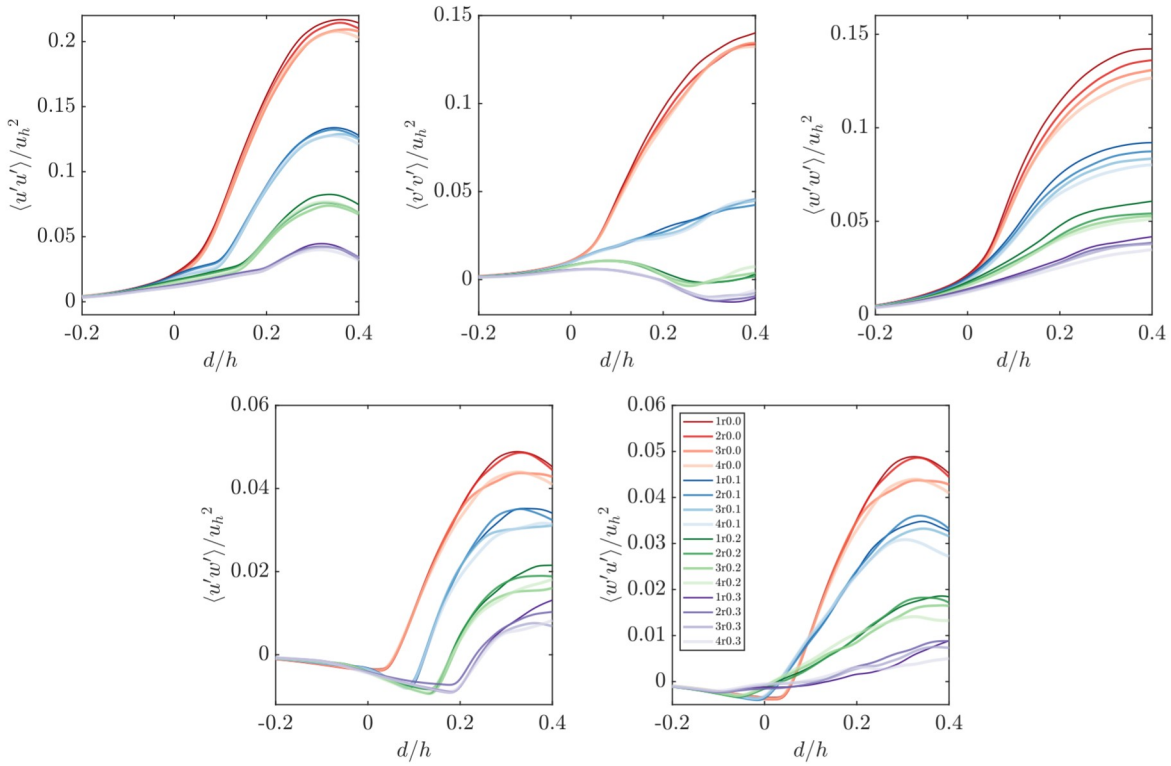

FIG. 11. Two-point correlation tensor components $\langle u_i' u_j' \rangle$ (see label) normalised with u_h^2 as a function of distance d/h from the interface for separation vectors $r/h = [0.0, 0.1, 0.2, 0.3]$ denoted by r0.0 to r0.3 in the legend respectively at times $t = [100, 120, 140, 160]$ denoted by 1 to 4 in the legend (first number) respectively. Positive d indicates the turbulent zone towards the centre of the jet. CV averaging is used.

behaviour is less relevant in the vertical fluctuation w'.

Figure 11 shows the four Reynolds-stress components discussed previously, with the addition of $\langle w'u' \rangle$ since $\langle w'u' \rangle \neq \langle u'w' \rangle$ for $r > 0$, calculated using CV averaging. The first letter in the correlation denotes the variable that is taken in the non-turbulent region. Each component is plotted against distance d/h for different separations r/h, represented by different colours, at times $t = [100, 120, 140, 160]$, represented by different line styles. All plots collapse in time (except for a negligible difference for some separations towards the jet centerline for components $\langle u'w' \rangle$ and $\langle w'u' \rangle$) showing that self-similarity is maintained for two-point correlations ($r/h \neq 0$). For the sake of clarity, we stress that the curves at $r/h = 0$ reported in figure 11 are the ones already discussed in figure 8. As expected, in all cases the correlation level decreases as r/h increases. The trend for most plots is similar

to the one-point statistics, that is, the largest correlation magnitude is reached towards the jet core. The only exception is $\langle v'v' \rangle$ which rapidly decreases as r/h increases and reaches negative values towards the jet core for $r/h \geq 0.2$. This behaviour differs with respect to the other two trace components, $\langle u'u' \rangle$ and $\langle w'w' \rangle$, which retain positive values as separation increases and their trends are similar to the $r/h = 0$ plots.

A particular behaviour amongst the trace components is seen for $\langle u'u' \rangle$. The plots for $r/h > 0$ increase linearly from the non-turbulent region, across the TNTI and into the turbulent region before abruptly increasing. The abrupt increase in the plot happens further into the turbulent region with increasing r/h. This means there is a region just below the TNTI where the correlation magnitude for $\langle u'u' \rangle$ increases at a constant rate with distance d/h for all separations. This behaviour is also present for the $\langle u'w' \rangle$ and $\langle w'u' \rangle$ components. In the latter case, the plots have decreasing negative values as they cross the TNTI into the turbulent region before abruptly increasing to positive values. Similarly to $\langle u'u' \rangle$, the sudden increase happens at higher d/h as r/h increases. The distance d/h at which these increases occur coincides for both $\langle u'u' \rangle$ and $\langle u'w' \rangle$. The same abrupt increase happens for $\langle w'u' \rangle$. Contrary to the previous two components, the increase begins in the non-turbulent region before the TNTI is reached. Only the plot at $r/h = 0$ increases inside the turbulent region. Even though $\langle u'w' \rangle$ and $\langle w'u' \rangle$ components are relatively small in magnitude compared to the trace components, they are nonetheless important contributions to the turbulence dynamics for their physical shear relevance. In particular it is worth mentioning that the change of sign that persists also in the two point correlation allows us to highlight that TNTI can pose a challenge also in the contest of LES models based on subgrid viscosity.

In the context of TNTIs, statistical averages vary when conditioned on the interface, which significantly affects the perception and calculation of turbulence statistics. Variations between the correlations of different velocity fluctuation components also highlight the non-homogeneity and non-isotropic nature of the flow.

IV. CONCLUSIONS

The velocity fluctuation correlations from the direct numerical simulation data of a planar turbulent temporal jet were analysed. Both one-point correlations, that is the classical Reynolds-stress tensor components, and two-point correlations were considered. The latter

were considered in the two-dimensional space of distance from the TNTI and separation between the correlation points

Three types of averaging were considered. Firstly, a classical average was considered, taken with respect to a spatially averaged TNTI location. This was then compared to another two types averages taken conditionally to the instantaneous TNTI. Of the latter, one type traverses the TNTI in the vertical direction whilst the other type is taken normal to the TNTI. The conditional averages are found to be generally equal, thus removing the need of complex data processing to compute normals and interpolate data. On the other hand, the classical average is significantly different, especially around the TNTI region, with respect to the conditional averaging, over a distance which is comparable to the TNTI's probability density function standard deviation.

All the correlations considered scale in time when normalised with a characteristic jet width which is calculated from integral quantities of momentum and volume fluxes. The scaling in time and the similarity between conditional averages allowed the comparison of the different correlation components by considering a fixed time during the simulation and one of the conditional averages.

Negative correlations of $\langle u'w' \rangle$ show that the region near the TNTI exhibits counter-gradient momentum transport and local turbulence suppression, a behavior that challenges the assumptions of conventional turbulence models and suggests the need for appropriate modeling strategies that take into account the TNTI.

The multi-scale correlations were plotted in a two-dimensional framework of separation between the correlation points and physical distance from the TNTI. The location of relevant peaks clearly demonstrate that, even when studied in a conditional framework, the dynamics of the velocity fluctuations, with respect for example to enstrophy, shows the presence of lengths scales that are very large with respect to the width of the turbulent region. The conditional velocity correlation functions exhibit distinct peaks at well-defined separations, indicating the typical scales of turbulent motions influenced by the TNTI. These features are not captured in classical statistics or in prior TNTI studies relying solely on one-point quantities.

A specific type of correlation was considered where one point is always fixed on the TNTI whilst the other point moves into the turbulent zone as the separation increases. The correlation shows that the turbulent dynamics inside the turbulent zone are influenced by

the TNTI. The peak of these correlations are at scales similar to the probability density function standard deviation of the TNTI, suggesting that the deviation of the TNTI has a direct relation to the scales involved in the turbulence dynamics.

ACKNOWLEDGMENTS

The authors acknowledge the financial support of the Engineering and Physical Sciences Research Council (EPSRC) through the project "Multi-scale dynamics at the turbulent/non-turbulent interface of jets and plumes" - Grant EP/R042640/1. Computing time has been provided by the UK National Supercomputing Service ARCHER via the UK Turbulence Consortium (EPSRC grant EP/R029326/1).

---

[1] C. B. da Silva, J. C. R. Hunt, I. Eames, and J. Westerweel, Interfacial layers between regions of different turbulence intensity, Annual review of fluid mechanics **46**, 567 (2014).

[2] D. K. Bisset, J. C. R. Hunt, and M. M. Rogers, The turbulent/non-turbulent interface bounding a far wake, Journal of Fluid Mechanics **451**, 383 (2002).

[3] M. Holzner, A. Liberzon, N. Nikitin, W. Kinzelbach, and A. Tsinober, Small-scale aspects of flows in proximity of the turbulent/nonturbulent interface, Physics of fluids **19**, 071702 (2007).

[4] C. B. da Silva and J. C. F. Pereira, Invariants of the velocity-gradient, rate-of-strain, and rate-of-rotation tensors across the turbulent/nonturbulent interface in jets, Physics of fluids **20**, 55101 (2008).

[5] J. Mathew and A. J. Basu, Some characteristics of entrainment at a cylindrical turbulence boundary, Physics of Fluids **14**, 2065 (2002).

[6] J. Westerweel, C. Fukushima, J. Pedersen, and J. Hunt, Mechanics of the turbulent-nonturbulent interface of a jet, Physical review letters **95**, 174501 (2005).

[7] J. Westerweel, C. Fukushima, J. M. Pedersen, and J. C. R. Hunt, Momentum and scalar transport at the turbulent/non-turbulent interface of a jet, Journal of Fluid Mechanics **631**, 199 (2009).

[8] S. Corrsin and A. L. Kistler, *Free-stream boundaries of turbulent flows*, Tech. Rep. (Johns Hopkins University Baltimore, 1955).

[9] M. van Reeuwijk and M. Holzner, The turbulence boundary of a temporal jet, Journal of Fluid Mechanics **739**, 254 (2014).

[10] G. Borrell and J. Jiménez, Properties of the turbulent/non-turbulent interface in boundary layers, Journal of Fluid Mechanics **801**, 554 (2016).

[11] H. C. Burridge, D. A. Parker, E. S. Kruger, J. L. Partridge, and P. F. Linden, Conditional sampling of a high Péclet number turbulent plume and the implications for entrainment, Journal of Fluid Mechanics **823**, 26 (2017).

[12] R. R. Taveira and C. B. da Silva, Kinetic energy budgets near the turbulent/nonturbulent interface in jets, Physics of Fluids **25** (2013).

[13] T. Watanabe, C. Da Silva, and K. Nagata, Scale-by-scale kinetic energy budget near the turbulent/nonturbulent interface, Physical Review Fluids **5**, 124610 (2020).

[14] T. S. Silva, M. Zecchetto, and C. B. da Silva, The scaling of the turbulent/non-turbulent interface at high reynolds numbers, Journal of Fluid Mechanics **843**, 156 (2018).

[15] T. Watanabe, C. B. da Silva, Y. Sakai, K. Nagata, and T. Hayase, Lagrangian properties of the entrainment across turbulent/non-turbulent interface layers, Physics of Fluids **28**, 31701 (2016).

[16] M. Zecchetto and C. B. da Silva, Universality of small-scale motions within the turbulent/non-turbulent interface layer, Journal of Fluid Mechanics **916** (2021).

[17] M. van Reeuwijk, J. C. Vassilicos, and J. Craske, Unified description of turbulent entrainment, Journal of Fluid Mechanics **908** (2021).

[18] T. Ishihara, H. Ogasawara, and J. C. Hunt, Analysis of conditional statistics obtained near the turbulent/non-turbulent interface of turbulent boundary layers, Journal of Fluids and Structures **53**, 50 (2015).

[19] J. Philip, C. Meneveau, C. M. de Silva, and I. Marusic, Multiscale analysis of fluxes at the turbulent/non-turbulent interface in high reynolds number boundary layers, Physics of Fluids **26** (2014).

[20] T. Ishihara, Y. Kaneda, and J. C. Hunt, Thin shear layers in high reynolds number turbulence—dns results, Flow, turbulence and combustion **91**, 895 (2013).

[21] T. Watanabe, Y. Sakai, K. Nagata, Y. Ito, and T. Hayase, Enstrophy and passive scalar transport near the turbulent/non-turbulent interface in a turbulent planar jet flow, Physics of Fluids **26** (2014).

[22] A. Cimarelli, J.-P. Mollicone, M. van Reeuwijk, and E. De Angelis, Spatially evolving cascades in temporal planar jets, Journal of Fluid Mechanics **910** (2021).

[23] A. Cimarelli, A. Fregni, J.-P. Mollicone, M. van Reeuwijk, and E. De Angelis, Structure of turbulence in temporal planar jets, Physics of Fluids **34**, 045109 (2022).

[24] J. Craske and M. van Reeuwijk, Energy dispersion in turbulent jets. part 1. direct simulation of steady and unsteady jets, Journal of Fluid Mechanics **763**, 500 (2015).

[25] J. A. Redford, I. P. Castro, and G. N. Coleman, On the universality of turbulent axisymmetric wakes, Journal of Fluid Mechanics **710**, 419 (2012).

[26] L. Djenidi, R. Antonia, N. Lefeuvre, and J. Lemay, Complete self-preservation on the axis of a turbulent round jet, Journal of Fluid Mechanics **790**, 57 (2016).

[27] T. Watanabe, R. Jaulino, R. Taveira, C. da Silva, K. Nagata, and Y. Sakai, Role of an isolated eddy near the turbulent/non-turbulent interface layer, Physical Review Fluids **2**, 094607 (2017).